6166 *Macromolecules* **2010**, *43*, 6166–6173
DOI: 10.1021/ma100819j

Macromolecules
ARTICLE

Highly Structured Foams from Chitosan Gels

A. Testouri, C. Honorez, A. Barillec, D. Langevin, and W. Drenckhan*

Laboratoire de Physique des Solides, Université Paris-Sud, UMR8502 Orsay, France

Received April 15, 2010; Revised Manuscript Received June 1, 2010

ABSTRACT: We demonstrate how to generate highly ordered, solidified foam structures from chitosan hydrogels using millifluidic cross-flow techniques. In this, aqueous chitosan solutions (containing surfactant) and air are injected simultaneously at constant flow rates in a millimetric T-junction device, in which the gas thread breaks up to form extremely monodisperse bubbles. These bubbles travel along a tube in which the cross-linker glyoxal is added at constant flow rate via another T-junction in order to start the gelification of the chitosan. The bubbles are collected in appropriate devices, where they form hexagonally close-packed structures under the influence of gravity and/or confinement before the gelification process freezes the foam structure. The successful application of this technique requires the optimization of foam stability in conjunction with an appropriate choice of gelification time and the viscosity of the solution, both being strongly dependent on the chitosan concentration. Furthermore, reliable generation of monodisperse foams calls for a thorough calibration of the bubbling device for highly viscous and non-Newtonian fluids. Both aspects are presented here, relying in particular on rheological investigations, along with some resulting foam structures.

1. Introduction

Solid foams are composed of closely packed air bubbles integrated into a continuous solid phase. They have very versatile properties (lightness, low density, compressibility, high surface-to-volume ratio, high liquid adsorption capacity, etc.) and are used in a wide range of applications. The properties of solid foams are closely related to their density and their structure (bubble size and size distribution), which therefore need to be controlled with sufficient accuracy. We show here how this accuracy can be provided using aqueous polymer solutions in millifluidic cross-flow techniques to generate equal-volume bubbles which spontaneously organize into highly ordered (hexagonally close-packed) liquid foam structures under the influence of gravity or confinement, as shown in Figure 1. Once formed, these structures are solidified through the cross-linking of the polymer by an appropriate agent. We therefore benefit from a quasi-two-step process, in which an equilibrium liquid foam with well-controlled structural properties is formed, which subsequently solidifies.[1,2]

The polymer we use is *chitosan* (section 2), a biopolymer which is produced from chitin,[3−7] the most abundant natural polymer after cellulose. Chitosan forms biocompatible and biodegradable hydrogels via covalent reactions with dialdehyde groups (cross-linking). The cross-linker which we employ here is *glyoxal* (section 2).

Chitosan hydrogels have been widely studied and used for decades in different applications, including drug delivery, wound healing treatment, and thickening agents in the food industry.[7−10] Creating foams from these gels, especially sponge-like, open-cell foams, may greatly improve some of their properties such as high surface-to-volume ratio, an increased liquid absorption capacity, lightness despite a certain stiffness, or possible exchange with air. *Foamed* chitosan gels are already used in some applications such as wound bandage or tissue engineering.[7,8] The *controlled* foaming of hydrogels using micro- or millifluidic techniques has been attempted in recent years in particular for alginate gels[2,11,12] in a search for well-controlled material properties, for example toward scaffold development, in which pore-size control is a key parameter to ensure and optimize cell growth.[11,13]

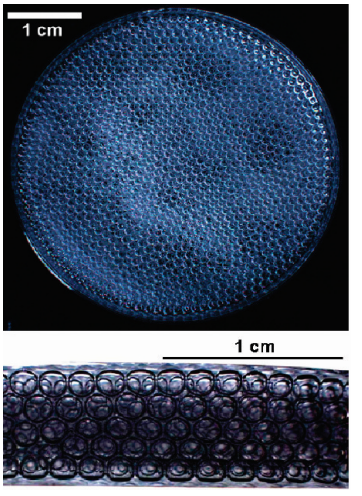

Figure 1. Examples of highly structured monodisperse, gelified chitsoan foams. Top: bubbles form close-packed, crystalline structures in a Petri dish due to gravity. Bottom: bubbles form close-packed structures due to confinement in a tube.

Reliable foam generation and solidification of polymer solutions are complex physicochemical processes, which are governed by a range of interdependent parameters, such as the (non-Newtonian) viscosity and gelification time of the polymer solution. We therefore performed a number of rheological (section 3), interfacial (section 4), and foaming (section 4) studies to choose appropriate chemical compositions and experimental conditions which provide sufficient time for foaming and sufficient foam stability before solidification. These investigations included the calibration of the millifluidic cross-flow device for our non-Newtonian

*To whom correspondence should be addressed.

 Published on Web 07/02/2010

solutions, which is presented in section 5. In section 6 we show some of the ordered gelified foam structures obtained after combining the results of the preinvestigations.

2. Materials and Methods

2.1. Materials and Preparation of the Polymer Solutions. Chitosan from crab shells was purchased from Sigma-Aldrich in powder form (CAS: 9012-76-4), with a medium molecular weight between 0.2×10^6 and 0.4×10^6 g/mol and a degree of deacetylation ranging between 75% and 85%. Chitosan is insoluble in most solvents, but the deacetylation allows it to become soluble in acidic[14,15] solutions by protonation of free amino groups as[16]

$$\mathrm{Chit}-\mathrm{NH_2} + \mathrm{H_3O^+} \leftrightarrows \mathrm{Chit}-\mathrm{NH_3^+} + \mathrm{H_2O}$$

The properties of chitosan solutions are strongly influenced by a range of parameters, such as the pH, the temperature, the molecular weight of the chitosan, and its degree of deacetylation.[17] In our case, the decisive parameter is the concentration C_{Ch} of the chitosan in the solution, which influences significantly the gelification kinetics and physical properties of the solutions, in particular their viscosity.

We prepared a chitosan stock solution of $C_{\mathrm{ch}} = 2$ wt % by dissolving the corresponding amount of chitosan in 0.1 mol/L acetic acid at 25 °C. Dissolution and homogenization were ensured by stirring for 48 h at room temperature. This stock solution was then diluted in 0.1 mol/L acetic acid to obtain a range of solutions with chitosan concentrations C_{ch} between 0.5 and 2.0 wt %. The pH of the chitosan solutions increased slightly with increasing chitosan concentration and was between 4 and 6.5.

In order to stabilize foams generated from these solutions, we added the surfactant Lutensol AT25 (fatty alcohol alkoxylate with a C16/C18 chain and a degree of ethoxylation of 25, $M = 1360$ g mol^{-1}, critical micellar concentration (cmc) in water $= 4.3 \times 10^{-6}$ mol L^{-1} [46]) provided by BASF. AT25 is a nonionic surfactant chosen to avoid electrostatic interactions between the charged chitosan and the surfactant. After a range of foaming tests, which are discussed in more detail in section 4, we decided to use an AT25 concentration of 0.59 wt % throughout the experiments, which corresponds to 1000 times the cmc in pure water.

The chitosan solutions are gelified using the organic compound glyoxal ($C_2H_2O_2$, 40% in water, CAS: 107-22-2), which was purchased from Sigma-Aldrich. Following the protocol provided by Payet,[18] we added the glyoxal at a proportion of 20 μL for 5 g of chitosan.

2.2. Methods and Procedures. *Rheology*. In order to characterize the bulk physical properties of the solutions and their gelification behavior (section 3), we used a rheometer (Physica MCR 300, Anton Paar, Germany) equipped with a cone−plate geometry (cone CP50-2: cone angle: 2°, diameter: 49.96 mm, truncation: 48 μm) in continuous and oscillatory mode, respectively. A trap was used to prevent evaporation of solvent during the measurements. The temperature was kept constant at 23 °C, using a thermostated bath. For investigation of the gelification times, the solutions are homogenized using a magnetic stirrer for 30 s after the glyoxal was added using the concentrations described in section 2.1.

Interfacial Tension. The interfacial tension (section 4) was measured using the Wilhelmy technique (NYMA) and cross-checked using a pendant drop device (Tracker from TECLIS). Since equilibration times can be quite long (up to 4 h) in the presence of chitosan, we conduct the measurements in a sealed container to avoid evaporation.

Foaming. Initial foamability tests were performed by hand-shaking the solutions violently in a closed container for 1 min and by imaging how the resulting foam decays with time (section 4).

The setup for the generation of monodisperse and gelifying foams, whose functioning is discussed in more detail in section 5, contains three syringe pumps (KdScientific KDS-100-CE with Becton Dickson seringes) to provide constant gas and liquid flow rates. The syringe pumps are connected to the foaming device, for which we use either commercial Kynar T-junctions (Kynar T-junction with an inner channel diameter of 1.25 mm and circular cross sections and Tygon R-3603 tubing with an internal diameter of 1.6 mm from Fisher Scientific) or T-junctions built in-house using high-precision drilling in polycarbon blocks for better visibility of the bubble generation process.

Bubble diameters are measured by taking images of several monolayers of bubbles organized in a close-packed hexagonal lattice and by measuring several times the length of an array of 5−10 bubbles.

Imaging. Foams and bubbles are imaged using different cameras from Allied Vision Technologies (Marlin CCD camera) and a VDS Vosskuhler high-speed high-resolution CMOS camera (up to 500 frames/s).

3. Characterization of Chitosan Solutions

Successful generation of monodisperse, ordered foam structures is largely controlled by the interplay between the gelification time τ_g and the viscosity η of the chitosan solutions. Since both parameters are simultaneously and strongly coupled to the chitosan concentration C_{Ch}, we determine these relationships here in more detail with the aim to choose a range of appropriate concentrations, which simultaneously provide (i) sufficiently *rapid gelification* to avoid foam breakage before solidification, (ii) sufficiently *slow gelification* to avoid blocking the foaming device and to allow the bubbles to self-organize in the foam before substantial solidification sets in, (iii) sufficiently *high viscosities* to enhance foam stability, and (iv) sufficiently *low viscosities* to ensure the reliable generation of equal-volume bubbles and to allow their self-organization within the foam.

To determine the viscous and gelification behavior of the solutions, we use a cone−plate rheometer (section 2.2), which is used in continuous rotation mode for the measurements of the viscosity and in oscillating mode for the measurement of the gelification time.

3.1. Viscous Properties of Nongelified Chitosan Solutions. All measurements were carried out over a range of shear rates $\dot{\gamma}$ (from 0.1 to 100 s^{-1}) and for chitosan concentrations between 0.3 and 2 wt %. We find that the viscosity of concentrated chitosan solutions decreases non-negligibly with time even at *constant shear rate*. As a result, the values for higher concentrations and higher shear rates are expected to depend on our measuring protocol. Since our principal interest here lies in the viscosity in the limit of zero shear rate (η_0) and a characterization of the general behavior of the chitosan solutions corresponding to our experimental conditions (in terms of typical shear rates and characteristic flow times), we decided on the following protocol: we measure at a small number of shear rates only, starting at the lowest shear rate (range 0.1−100 s^{-1}) with a fixed measurement time of 1000 s per data point.

Figure 2 shows how the viscosity η changes under these measuring conditions as a function of shear rate $\dot{\gamma}$ for a selection of chitosan concentrations ($C_{\mathrm{Ch}} = 0.9$, 1.5, 1.7, 1.9, and 2 wt %). We notice first of all that the viscosities of the solutions depend dramatically on the chitosan concentration, changing over almost 4 orders of magnitude as the concentration is increased from 0% (pure water $\eta = 0.001$ Pa s) to only 2% wt ($\eta \sim 6$ Pa s). Furthermore, with increasing chitosan concentration the solutions display an increasingly shear-thinning (i.e., non-Newtonian) behavior.[17−19] These properties indicate strong interactions between the polymers and long relaxation times, respectively, having important

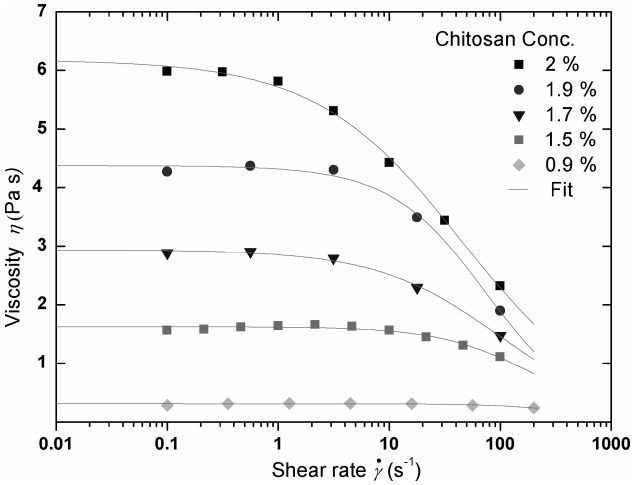

Figure 2. Viscosity as a function of shear rate $\dot{\gamma}$ for different chitosan concentrations.

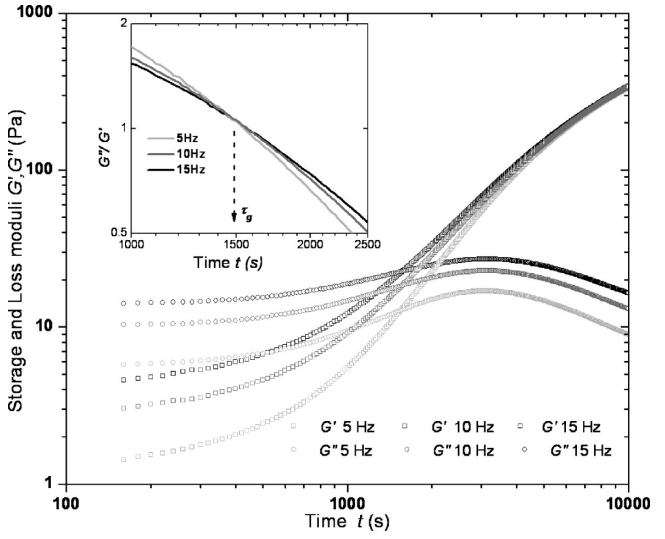

Figure 3. A typical example (chitosan concentration C_{Ch} = 1.6 wt %) of how the elastic and viscous moduli, G' and G'', respectively, change upon gelification at different excitation frequencies. Inset: plotting G''/G' provides a unique crossover point at the gelification point and hence a well-defined (frequency-independent) measure of the gelification time.

consequences on the generation of bubbles in millifluidic devices (section 5). As seen in Figure 2, Newtonian behavior is recovered for all solutions in the limit of low shear rates. We determine the zero-shear rate viscosities η_0 by fitting the data to the "Cross equation",[20−22] which is commonly used to describe the behavior of polysaccharide solutions:

$$\eta = \eta_\infty - \frac{\eta_0 - \eta_\infty}{1 + (a\dot{\gamma})^p} \quad (1)$$

Here η_∞ is the viscosity in the limit of very high shear rates, for which we use the viscosity of water (i.e., η_∞ = 0.001 Pa s). a corresponds to the polymer relaxation time, and p is a positive exponent. The resulting fits are shown along with the data in Figure 2, while the resulting zero-shear viscosities η_0 for the whole range of our measurements are shown in Figure 4 together with the gelification time τ_g (which is discussed in the next section).

The η_0 data are fitted well by a single power law:

$$\eta_0 \propto AC^B \quad (2)$$

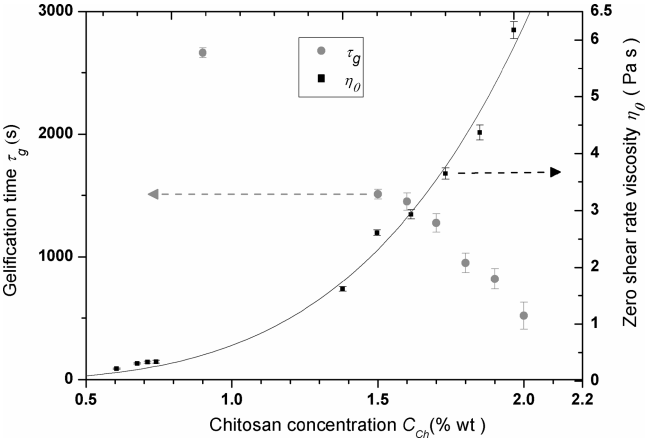

Figure 4. Gelification time τ_g and zero shear rate viscosity η_0 as a function of chitosan concentration C_{Ch}. The viscosity is fitted by eq 2 with $A = 0.32 \pm 0.05$ Pa s and $B = 4.2 \pm 0.3$.

with $A = 0.32 \pm 0.05$ Pa s and $B = 4.2 \pm 0.3$. The exponent of 4.2 is much higher than what is expected for polyelectrolyte solutions ($B \leq 1.5$).[23] The reasons for this are manifold. First of all, the ionic strength of our solutions (≈ 0.1 M) is sufficiently large to have Debye lengths of the order of 1 nm, meaning that charges are strongly screened and that the polymers interact more like neutral polymers. However, even for neutral polymers in the concentrated, entangled regime standard reptation theory predicts that $B \leq 15/4$.[24] This additional deviation for chitosan solutions has been discussed intensively in the recent literature (ref 25 and references therein) and is now commonly assigned to the fact that chitosan molecules experience additional (attractive) interactions which are not taken into account in standard reptation models. Of particular importance is the effect of hydrogen-bonding and hydrophobic interactions[26] requiring the consideration of "sticky-reptation"-type models[27] which predict exponents of up to 8.5.

Comparison with chitosan solutions investigated under similar conditions in the literature[18,25] also allows us to conclude that our measurements are done for a range of chitosan concentrations corresponding to the concentrated, entangled regime, hence justifying the fact that they are well described by a single power law.

3.2. Gelification Time τ_g. In order to determine the gelification time τ_g of the chitosan solutions in the presence of glyoxal, we follow the gelification process by determining the elastic and viscous modulus (G' and G'', respectively) of the samples as a function of time t after the injection and homogenization of glyoxal. For details of the solution preparation and the rheometer see section 2.2.

A typical example for a chitosan concentration of 1.6 wt % at excitation frequencies of 5, 10, and 15 Hz is shown in Figure 3. The curves show for each frequency the classical behavior of solidification: while the viscous modulus G'' goes through a small maximum, the elastic modulus G' increases significantly with time to reach a plateau when the solidification process terminates. The crossover of both curves is generally taken as the gelification point, since at this point the material goes from one dominated by viscous behavior to one dominated by elastic behavior. This crossover is, however, sensitive to the excitation frequency, which is why we preferred to follow the approach suggested by Chambon et al. and successfully employed for chitosan gelification:[18,28−30] Following from the fact that the material structure becomes scale-invariant at the gelification point, the ratio of the viscous and the elastic modulus G''/G' is

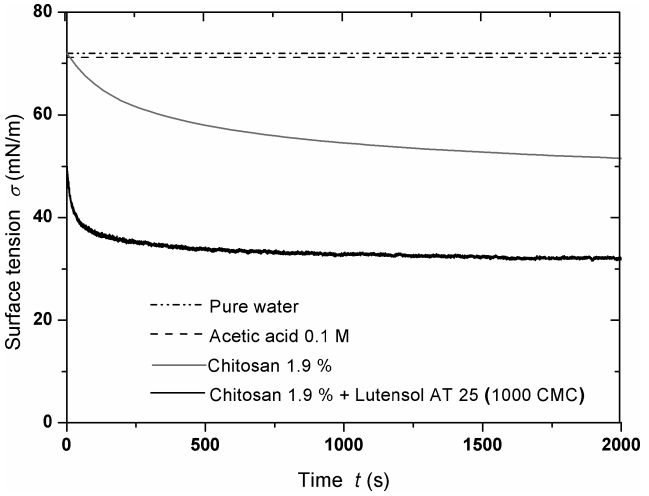

Figure 5. Evolution of the surface tension σ of a rapidly generated gas/liquid interface ("rising bubble" in the TRACKER device) for pure water, our acid/water mixture (sketched), our standard chitosan solution (C_{Ch} = 1.9 wt %), and the chitosan solution with added surfactant (1000·cmc of AT25).

independent of the excitation frequency at τ_g. This means that considering G''/G' as a function of time provides a unique crossover of all curves at τ_g. An example of a resulting curve is shown in the inset of Figure 3 for the chitosan concentration of 1.6 wt % with a crossover at $G''/G' = 1.05$ at $\tau_g \approx 1500$ s.

Using this approach, we determine the gelification time τ_g for a range of chitosan concentrations. The results are displayed together with the zero shear rate viscosities η_0 in Figure 4. This figure allows us to choose an appropriate window of chitosan concentrations based on the requirements of the foaming process, which are discussed in more detail in sections 4 and 5. In our case we decided to work with a chitosan concentration of C_{Ch} = 1.9 wt %, which provides us with a gelification time of $\tau_g = 820 \pm 80$ s and a zero shear rate viscosity of $\eta_0 = 4.37 \pm 0.13$ Pa s.

4. Optimization of Foamability and Foam Stability

In order to stabilize the foams against coalescence, an appropriate surface-active stabilizer needs to be chosen. Already the chitosan by itself, under the conditions used by us (section 2.1), appears as highly surface active. This fact is illustrated in Figure 5, where we show how the surface tension σ of our standard chitosan solution (1.9 wt % chitosan in 0.1 mol/L acetic acid) changes as a function of time after rapid generation of a gas/liquid interface (Tracker device, section 2.2). While the surface tension of pure water and the water/acid mixture remains literally unchanged with time (72 and 71 mN/m, respectively, sketched in Figure 5), that of the chitosan solution drops significantly but slowly to about 52 N/m, indicating the slow arrival of surface active species at the interface. This observation is confirmed by the fact that reasonably stable foams can be generated from these chitosan solutions without adding any additional surfactants. This could be due to the presence of surface active impurities in the chitosan powder, but we believe it to be a true effect of the hydrophobicity of the chitosan. First, with a degree of deacetylation between 75 and 85%, the chitosan molecules contain significant hydrophobic sections. Second, a low pH is required to sufficiently protonate the amino groups of the chitosan to render the remaining parts hydrophilic. In our case, we find a pH of 6−6.5 for the highly concentrated chitosan solutions, meaning that the free amino groups become less protonated, leading to a further increase of hydrophobicity of the chitosan chains and

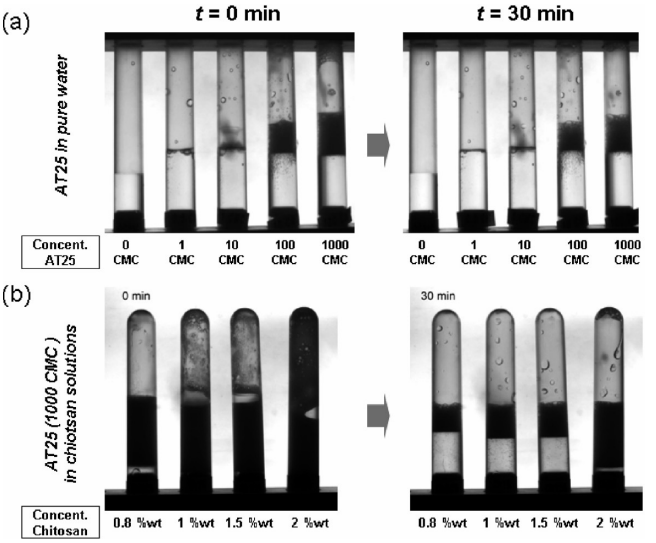

Figure 6. Foamability (left, t = 0 min) and foam stability (right, t = 30 min) of (a) aqueous solutions of the surfactant AT25 expressed as multiples of the critical micellar concentration (cmc = 4.3×10^{-6} mol L^{-1}) and (b) chitosan solutions with increasing chitosan concentration at constant surfactant concentration (AT25 at 1000·cmc).

hence a strong surface activity.[31] The tendency of the molecules to arrange their hydrophobic and hydrophilic parts at the gas−liquid interface may be further enhanced by the fact that electrostatic intramolecule interactions are strongly screened in our solutions (section 3), providing therefore more flexible polymer chains.

The typical equilibration times of the chitosan-enriched interfaces are of the order of 10 min (Figure 5), which is too slow for our foaming process, in which foams of closely packed bubbles are generated within a few seconds, and in which the coalescence of bubbles needs to be absolutely avoided to maintain the monodispersity and ordered structure of the final foam. We therefore add a low-molecular-weight surfactant, which, on average and at sufficiently high surfactant concentration, diffuses to the interface in a few milliseconds. Since the chitosan is charged, we chose the nonionic surfactant Lutensol AT25 (section 2.1) for this purpose. As shown in Figure 5, the addition of this surfactant at a concentration of 0.59 wt % (which corresponds to 1000 times its cmc in pure water) not only decreases further the surface tension (42 mN/m) but also greatly accelerates the main decrease to a few seconds.

Since the AT25 has a very low critical micellar concentration (cmc = 4.3×10^{-6} mol/L in pure water), reasonably large surfactant concentrations need to be used to ensure that all the interfaces in a foam can be covered sufficiently (and sufficiently quickly) to ensure foam stability. This is due to the fact that foams have a very large surface to volume ratio. In order to choose the appropriate surfactant concentration, we performed simple foaming tests by shaking (section 2.1) for a range of concentrations of AT25 in pure water. Results are shown in Figure 6a, where the left image, taken immediately after shaking the tubes (t = 0 min), provides an indication of the foamability, while the right image, taken after 30 min (t = 30 min), provides an indication of the foam stability over a period relevant to our typical experimental time scale. It is obvious from these results that very high concentrations of AT25 are required to ensure both foamability and foam stability, which is why we fixed the working concentration at C_{AT25} = 1000·cmc (corresponding to 0.59 wt %).

Since the presence of the chitosan increases significantly the viscosity of the solution, the foams are stabilized additionally by the fact that gravity-driven drainage of liquid is reduced sufficiently to avoid the otherwise rapid formation of thin films which are very sensitive to rupture. This is illustrated in Figure 6b, which

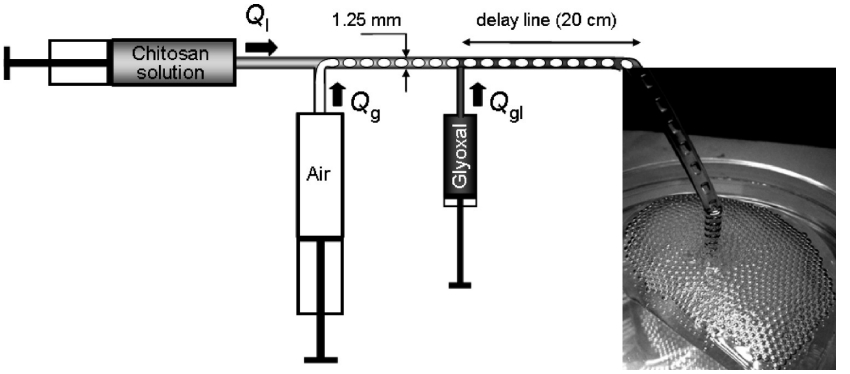

Figure 7. Setup to generate the monodisperse foams: two syringe pumps deliver the chitosan solution and air at constant flow rate into a T-junction, where the gas thread breaks up into extremely monodisperse bubbles. These travel further down a tube where a second T-junction is used to inject the glyoxal solutions (here: $Q_g = Q_l = 25$ mL/h, $Q_{gl} = 2.5$ mL/h, $C_{CH} = 1.9$ wt % + 0.59 wt % AT25). A "delay line" of 20 cm allows the glyoxal to diffuse into the solution before the foam exits the tube and is collected in appropriate dishes.

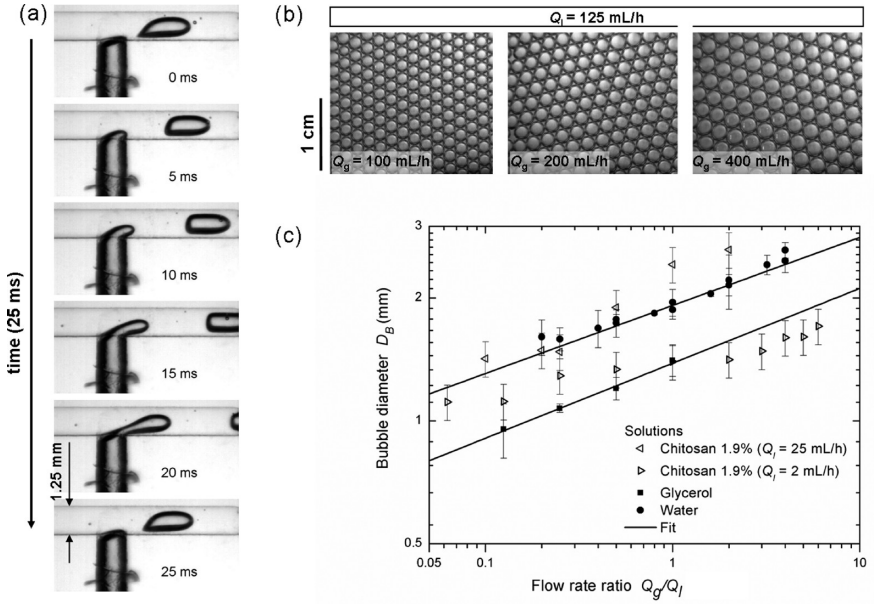

Figure 8. (a) One period of the bubble generation in the T-junction device for the glycerol/surfactant mixture ($Q_g = Q_l = 30$ mL/h). (b) Resulting bubbles for water/surfactant solution for increasing gas flow rates Q_g. (c) Calibration of the T-junction: for the Newtonian solutions (water and glycerol + 0.59 wt % AT25), the relationship between the bubble diameter D_B and the flow rate ratio Q_g/Q_l is well described by a power law (eq 3 with: water: $\alpha = 1.92 \pm 0.02$ mm, $\beta = 0.17 \pm 0.01$; glycerol: $\alpha = 1.38 \pm 0.02$ mm, $\beta = 0.18 \pm 0.01$). This is not the case for the strongly shear-thinning chitosan solutions (here $C_{CH} = 1.9$ wt % + 0.59 wt % AT25), for which the absolute liquid flow rate Q_l is also a decisive parameter.

shows how foamability and foam stability improve with increasing chitosan concentration for a constant surfactant concentration (1000·cmc).

5. Monodisperse Foam Generation

5.1. Bubble Generation. As sketched in Figure 7, we generate highly monodisperse foams (polydispersity < 5%) using a millifluidic technique in which the foaming solution and air are injected simultaneously and at constant flow rates (Q_l and Q_g, respectively), into two neighboring branches of a T-junction.[32,33] When working in the right flow rate ranges (in our case both flow rates are of the order of 1−100 mL/h), the forming gas thread is pinched off by the liquid flow in an extremely regular manner, producing very monodisperse bubbles entrained by a well-defined amount of liquid, which sets the total liquid content ϕ of the created foam to $\phi = Q_l/(Q_l + Q_g)$. One period of the periodic bubbling process is shown in Figure 8a and typical images of obtained bubbles in Figure 8b. The diameter of the generated bubbles is of the order of the geometric dimensions of the T-junction, which in our case are chosen millimetric (all three channels have a diameter of 1.25 mm) to facilitate the device manufacture but can be driven down to smaller dimensions.[32] Moreover, as in other device geometries, the bubble diameter and the final liquid content can be controlled elegantly by adjusting the ratio of the flow rates[34−37] and bubble production rate can be driven up to a few hundred bubbles per second.

We calibrated our T-junction device with two reference solutions: pure water ($\eta = 0.001$ Pa s) and pure glycerol ($\eta = 1.5$ Pa s), both containing the surfactant AT25 at a concentration of 1000·cmc. The surface tension of both solutions is close to 45 mN/m. The resulting bubble sizes (diameter D_B) are found to be highly reproducible and are shown in Figure 8c as a function of flow rate ratio Q_g/Q_l. Each data point consists of data taken for different liquid and gas flow rates keeping their ratio constant (50 mL/h < Q_l < 125 mL/h; 10 mL/h < Q_g < 400 mL/h). As is found for many different device geometries,[34−38] our data are well captured by a simple power law

$$D_B = \alpha\left(\frac{Q_g}{Q_l}\right)^{\beta} \quad (3)$$

with $\alpha = 1.92 \pm 0.02$ mm and $\beta = 0.17 \pm 0.01$ for the case of water and $\alpha = 1.38 \pm 0.02$ mm and $\beta = 0.18 \pm 0.01$ for the case of glycerol. While the exponent remains virtually unchanged, the prefactor drops in the case of glycerol due to the increased viscosity.

For the moment, we are not able to rationalize quantitatively either the measured exponent or the prefactor of this scaling. Intensive research over the past few years has established that the generation of monodisperse bubbles and droplets in these kinds of devices falls into three main flow-condition-dependent regimes: the squeezing regime, the dripping regime, and the jetting regime.[34−37,39] The squeezing regime is pressure-driven[32] and occurs at low capillary numbers ($Ca = \eta U/\gamma \ll 1$, with U being the liquid velocity) and for confined bubbles, which block the channel. Bubble sizes in the squeezing regime are commonly found to be independent of the liquid viscosity and the interfacial tension and are well described by $D_B \sim (Q_g/Q_l)^{1/3}$.[34−37,39] For increasing capillary number ($Ca \approx 1$, dripping regime), viscous forces start to play a role in bubble detachment and the bubble size becomes (also) a function of the capillary number. If the bubbles are much smaller than the channel, i.e., if they can be considered as unconfined, the bubble size becomes a function of the capillary number only. The jetting regime occurs when inertial forces start playing a role (high Reynolds number), which is not the case here.

Calculating typical capillary numbers for our cases (water: $10^{-4} < Ca < 10^{-3}$; glycerol: $Ca \approx 1$) and considering the typical bubble sizes/shapes in the channel (Figure 8a), we see that we happen to be between the squeezing and the dripping regime, having as a consequence, that bubble sizes depend on the flow rate ratio *and* on the liquid viscosity. Quantitative comparison with previously established results is also rendered difficult by the fact that most previous work has been done in channels with flat, rectangular cross sections, which do not only have a quasi-two-dimensional geometry but also corners through which liquid may flow more easily. We will therefore refrain from any more detailed comparison here but remind the reader that the device can be very well calibrated for Newtonian liquids, as is obvious from Figure 8c.

Unfortunately, this is less straightforward for non-Newtonian liquids, such as the chitosan solutions employed here. Figure 8a shows two data sets for our standard chitosan solution ($C_{Ch} = 1.9$ wt %) for two different liquid flow rates $Q_l = 2$ mL/h and $Q_l = 25$ mL/h (only the gas flow rate Q_g is varied in each curve). Unlike in the case of Newtonian liquids, the data cannot be collapsed in order to be expressed as a function of the flow rate ratio Q_g/Q_l only, but depends strongly on the absolute liquid flow rate Q_l. This is a natural consequence of the strongly non-Newtonian flow behavior of such highly concentrated chitosan solutions subjected to the flow conditions in the T-junction device. The flow of the solution being confined to the liquid film formed between the wall and the bubble surface leads to shear rates $\dot{\gamma}$ of the order of $10-1000\ s^{-1}$ (assuming a film thickness of the order of $100\ \mu$m). Comparing this with the viscosity results of Figure 2, we see that in this regime the chitosan solution is extremely shear thinning. One would therefore expect that bubble sizes increase with increasing liquid flow rate. The same general argument may also explain why the slope cannot be the same as that of Newtonian liquids: changing the gas flow rate Q_g changes the confinement of the liquid flow and therefore its local shear rate.

However, as in the case for the Newtonian solutions, we find that the calibration of the chitosan solutions is sufficiently reliable from an experimental point of view, meaning that if care is taken to work always under the same conditions, the generated bubble sizes are very monodisperse and reproducible.

Table 1.

parameter	value
chitosan concentration C_{Ch}	1.9 wt %
concentration of glyoxal solution	0.16 wt %
liquid flow rate Ql	25 mL/h
gas flow rate Qg	25 mL/h
glyoxal flow rate Q_{gly}	2.5 mL/h
T-junction diameter	1.5 mm
temperature	20−23 °C
tube length	20 cm

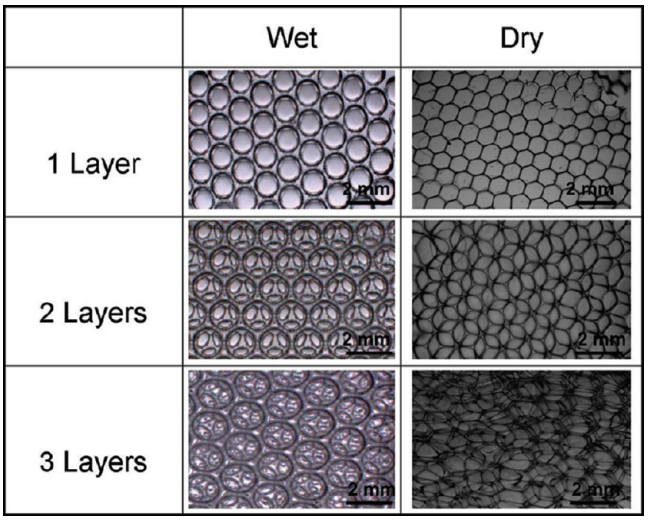

Figure 9. Close-up examples of obtained foam structures in the wet state immediately after gelification and when dried at the open air.

5.2. Gelification. In order to gelify the foam we add another T-junction just after the bubble generation (Figure 7) where we inject a diluted glyoxal solution (0.16 wt %) at constant flow rate Q_{gl}, calculated to reproduce the same conditions used for the measurements of the gelification time τ_g in section 3. To allow the glyoxal to diffuse into the liquid, we let the bubbles travel along a "delay line" of 20 cm. This also enhances significantly the stability of the final foam, which we collect in containers at the end of the delay line.

6. Structure of the Obtained Gelified Foam

All the samples demonstrated in this section are generated using the parameters given in Table 1. Some general examples of the obtained gelified foams are shown in Figures 1 and 7. In Figure 9 we show some close-up images of different numbers of hexagonally close-packed layers of bubbles spontaneously obtained by depositing the foams in Petri dishes. In the left column of Figure 9 we show what the foams look like just after gelification, i.e., containing the original amount of water. As the number of bubble layers increases, one sees clearly the appearance of three black rings in each bubble, which is an image of the three touching bubbles in the layer underneath.[40] The right column shows what these foams look like after they have been dried under ordinary room conditions for 24 h. While the wet foams are very robust gels, the dry ones become very brittle.

7. Conclusions and Outlook

We have demonstrated a simple technique that can be used to generate extremely monodisperse, ordered foam structures from chitosan gels using millifluidic cross-flow techniques. This article

puts an emphasis on the general introduction of the technique in conjunction with the characterization of the foaming properties and the gelifying behavior of the employed polymer. Future work should exploit in depth its potential to generate a range of foam structures of different bubble sizes and densities (spherical vs polehydral bubbles) and to explore in detail the physical properties of the obtained foams.

In order to obtain ordered bubble crystals, like the ones shown in Figure 9, one needs to work initially with foams that have a liquid content of more than 30% (random close-packing of spheres corresponds to 36%) to ensure that bubbles remain spherical and glide easily one past another to find their optimal location in the hexagonally close-packed structure. Ordered, gelified foams with lower liquid content and therefore with nonspherical bubbles can be formed by allowing the liquid to drain, either due to gravity or through the application of pressure gradients.[41] With highly viscous liquids, such as the chitosan solutions used here, this draining process takes time, which requires an even more delicate fine-tuning of foam stability and gelification time.

There should, however, also be a great interest in generating monodisperse chitosan foams with disordered structures. These can be achieved by tuning the liquid and gas flow rates in such a way as to produce immediately foams of low liquid fractions. In some preliminary tests we have seen that this may also be a promising route to generate open-cell foams. While the foams generated at high liquid content seem to maintain closed cells upon gelification, those containing a smaller amount of liquid and hence larger and thinner films separating the bubbles are more likely to experience film rupture upon gelification such that holes are created between bubbles, while the overall bubble structure is "frozen", leaving behind a sponge-like material.

The generation of gelified foams entrains two particularly interesting fundamental questions, which are already receiving increasing attention due to their relevance to applications: the first concerns the understanding of the functioning of a number of micro- or millifluidic techniques for non-Newtonian solutions. The second concerns the long-term "stability" of the gelified porous materials. For example, in some cases, we were not able to permanently "freeze" the gelified foam structures. In those cases the elastic modulus of the gel network was not sufficient to counterbalance pressure differences between bubbles, hence driving a self-amplifying gas exchange from the smaller to the bigger bubbles known as *foam coarsening*.[42] Important fundamental questions are therefore related to the existence of a limiting elasticity of the continuous phase to entirely stop the coarsening or, in more general terms, to the bubble size distribution obtained in a coarsening foam which has a non-negligible network elasticity. Similar questions have been posed for foams containing particles confined to the gas/liquid interface[43] or at high concentrations in the bulk liquid separating bubbles.[44]

Last but not least, we have seen that in the case of the surface active chitosan it is not necessary to add low-molecular-weight surface active agents if the delay line is sufficiently long to allow the chitosan molecules to arrive at the bubble surface (this process is probably accelerated by the shear between the bubbles and the solid tube walls) and to allow the reticulation to progress sufficiently to stabilize significantly the bubbles in the foam. This fact may be particularly interesting for biological or medical applications in which the integration of surfactants into the gel may pose a problem.

In very general terms, techniques of this kind should easily be transferable to a large range of polymers and reticulants. In the case of monomeric acrylamide solutions, which are polymerized and cross-linked simultaneously in the solidifying foam, this has been demonstrated by Van der Net et al.[1] Sang et al. successfully used physically cross-linked (ionic) alginate solutions containing ferrofluid particles to render the foamed gels stimulable.[2] In general, using milli- or microfluidic techniques for the well-controlled generation of multiphase systems with one solidifying component presents a very promising and versatile "lego-type" route to the fabrication of simple or complex materials with equally well-controlled properties. For example, the solidification of the continuous phase of monodisperse (and highly structured) foams, emulsions, or even multiple emulsions generates versatile porous materials (for example, for scaffolding[11]), while the polymerization of the discontinuous phase of (multiple) emulsions leads to efficient manufacture of monodisperse solid particles.[45]

Acknowledgment. We thank Alain Ponton for suggesting to use chitosan as a biopolymer for our purposes. We thank him and Valentin Leroy for the many discussions we had on this subject. We also thank Amelie Lecchi for her continuous support concerning chemical questions.

References and Notes

(1) Van der Net, A.; Gryson, A.; Ranft, M.; Elias, F.; Stubenrauch, C.; Drenckhan, W. Highly Structured Porous Solids from Liquid Foam Templates. *Colloids Surf., A* **2009**, *346*(1−3), 5−10.
(2) Yip Cheung Sang, Y. Vers des micromousses stimulables (Toward smart microfoams). In *MSC*; University of Denis Diderot Paris 7: Paris, 2009.
(3) Kim, I. Y.; Seo, S. J.; Moon, H. S.; Yoo, M. K.; Park, I. Y.; Kim, B. C.; Cho, C. S. Chitosan and its derivatives for tissue engineering applications. *Biotechnol. Adv.* **2008**, *26* (1), 1–21.
(4) Desbrieres, J. Viscosity of semiflexible chitosan solutions: Influence of concentration, temperature, and role of intermolecular interactions. *Biomacromolecules* **2002**, *3* (2), 342–349.
(5) Mucha, M. Rheological characteristics of semi-dilute chitosan solutions. *Macromol. Chem. Phys.* **1997**, *198* (3), 483.
(6) Koide, S. S. Chitin-chitosan: Properties, benefits and risks. *Nutr. Res.* (*N.Y.*) **1998**, *18* (6), 1091–1101.
(7) Rinaudo, M. Chitin and chitosan: Properties and applications. *Prog. Polym. Sci.* **2006**, *31* (7), 603–632.
(8) Choi, S. W.; Xie, J. W.; Xia, Y. N. Chitosan-Based Inverse Opals: Three-Dimensional Scaffolds with Uniform Pore Structures for Cell Culture. *Adv. Mater.* **2009**, *21* (29), 2997.
(9) Chenite, A.; Buschmann, M.; Wang, D.; Chaput, C.; Kandani, N. Rheological characterisation of thermogelling chitosan/glycerol-phosphate solutions. *Carbohydr. Polym.* **2001**, *46* (1), 39–47.
(10) Han, H. D.; Nam, D. E.; Seo, D. H.; Kim, T. W.; Shin, B. C.; Choi, H. S. Preparation and biodegradation of thermosensitive chitosan hydrogel as a function of pH and temperature. *Macromol. Res.* **2004**, *12* (5), 507–511.
(11) Chung, K. Y.; Mishra, N. C.; Wang, C. C.; Lin, F. H.; Lin, K. H. Fabricating scaffolds by microfluidics. *Biomicrofluidics* **2009**, *3* (2).
(12) Barbetta, A.; Gumiero, A.; Pecci, R.; Bedini, R.; Dentini, M. Gas-in-Liquid Foam Templating as a Method for the Production of Highly Porous Scaffolds. *Biomacromolecules* **2009**, *10* (12), 3188–3192.
(13) Sung-Wook, C.; Jingwei, X.; Younan, X. Chitosan-Based Inverse Opals: Three-Dimensional Scaffolds with Uniform Pore Structures for Cell Culture. *Adv. Mater.* **2009**, *21* (29), 2997–3001.
(14) Babak, V.; Lukina, I.; Vikhoreva, G.; Desbrieres, J.; Rinaudo, M. Interfacial properties of dynamic association between chitin derivatives and surfactants. *Colloids Surf., A* **1999**, *147* (1−2), 139–148.
(15) Kjoniksen, A. L.; Nystrom, B.; Iversen, C.; Nakken, T.; Palmgren, O.; Tande, T. Viscosity of dilute aqueous solutions of hydrophobically modified chitosan and its unmodified analogue at different conditions of salt and surfactant concentrations. *Langmuir* **1997**, *13* (19), 4948–4952.
(16) Payet, L.; P., A.; Agnely, F.; Colinart, P.; Grossiord, J. L. Caractérisation rhéologique de la gélification d'alginate et de chitosane: effet de la température. *Rhéologie* **2002**, *2*, 46–51.
(17) Martinez, A.; Chornet, E.; Rodrigue, D. Steady-shear rheology of concentrated chitosan solutions. *J. Texture Stud.* **2004**, *35* (1), 53–74.
(18) Payet, L. *Viscoelasticite et structure de gels a base de chitosane*; Universite Paris 7: Paris, 2005.
(19) Desbrieres, J.; Bousquet, C.; Babak, V. G. Interfacial properties of ionic amphiphilic systems based on polysaccharides. *Rev. Roumaine Chim.* **2007**, *52* (4), 423.

(20) Kluge, T.; Masuda, A.; Yamashita, K.; Ushida, K. Concentration and molecular weight dependence of the quenching of Ru(bpy)(3)-(2+) by ferricyanide in aqueous solutions of synthetic hyaluronan. *Macromolecules* **2000**, *33* (2), 375–381.
(21) Ren, Y.; Ellis, P. R.; Ross-Murphy, S. B.; Wang, Q.; Wood, P. J. Dilute and semi-dilute solution properties of (1 → 3), (1 → 4)-beta-D-glucan, the endospenn cell wall polysaccharide of oats (Avena sativa L.). *Carbohydr. Polym.* **2003**, *53* (4), 401–408.
(22) Ren, Y. L.; Ellis, P. R.; Sutherland, I. W.; Ross-Murphy, S. B. Dilute and semi-dilute solution properties of an exopolysaccharide from Escherichia coli strain S61. *Carbohydr. Polym.* **2003**, *52* (2), 189–195.
(23) de Gennes, P. G.; P., P.; Velasco, R. M.; Brochard, F. Remarks on polyelectrolyte conformation. *J. Phys.* (*Paris*) **1976**, *37*, 1461–1473.
(24) de Gennes, P. G. *Scaling Concepts in Polymer Physics*; Cornell University Press: Ithaca, NY, 1979.
(25) Cho, J.; Heuzey, M.-C.; Bégin, A.; Carreau, P. J. Viscoelastic properties of chitosan solutions: Effect of concentration and ionic strength. *J. Food Eng.* **2006**, *74* (4), 500–515.
(26) Muthukumar, M. Dynamics of polyelectrolyte solutions. *J. Chem. Phys.* **1997**, *107* (7), 2619–2635.
(27) Rubinstein, M.; Semenov, A. N. Dynamics of entangled solutions of associating polymers. *Macromolecules* **2001**, *34* (4), 1058–1068.
(28) Chambon, F.; W., H. Linear viscoelasticity at the gel point of a crosslinking PDMS with imbalanced stoichiometry. *J. Rheol.* **1987**, *31* (8), 683–697.
(29) Moura, M. J.; Figueiredo, M. M.; Gil, M. H. Rheological Study of Genipin Cross-Linked Chitosan Hydrogels. *Biomacromolecules* **2007**, *8* (12), 3823–3829.
(30) Mours, M.; Winter, H. H. Relaxation patterns of nearly critical gels. *Macromolecules* **1996**, *29* (22), 7221–7229.
(31) Elsabee, M. Z.; Morsi, R. E.; Al-Sabagh, A. M. Surface active properties of chitosan and its derivatives. *Colloids Surf., B* **2009**, *74* (1), 1–16.
(32) Garstecki, P.; Fuerstman, M. J.; Stone, H. A.; Whitesides, G. M. Formation of droplets and bubbles in a microfluidic T-junction - scaling and mechanism of break-up. *Lab Chip* **2006**, *6* (5), 693–693.
(33) Xu, J. H.; Li, S.; Chen, G. G.; Luo, G. S. Formation of monodisperse microbubbles in a microfluidic device. *AIChE J.* **2006**, *52*, 2254–2259.
(34) Christopher, G. F.; Anna, S. L. Microfluidic methods for generating continuous droplet streams. *J. Phys. D: Appl. Phys.* **2007**, *40*, R319–R336.
(35) Garstecki, P.; Gitlin, I.; DiLuzio, W.; Whitesides, G. M.; Kumacheva, E.; Stone, H. A. Formation of monodisperse bubbles in a microfluidic flow-focusing device. *Appl. Phys. Lett.* **2004**, *85*, 2649–2651.
(36) Lorenceau, E.; Sang, Y. Y. C.; Hoehler, R.; Cohen-Addad, S. A high rate flow-focusing foam generator. *Phys. Fluids* **2006**, *18* (9), 097103.
(37) Marmottant, P.; Raven, J. P. Microfluidics with foams. *Soft Matter* **2009**, *5* (18), 3385–3388.
(38) Martinez, C. J. Bubble generation in microfluidic devices. *Bubble Sci., Eng. Technol.* **2009**, *1* (1−2), 40–52.
(39) De Menech, M.; Garstecki, P.; Jousse, F.; Stone, H. A. Transition from squeezing to dripping in a microfluidic T-shaped junction. *J. Fluid Mech.* **2008**, *595* (1), 141–161.
(40) van der Net, A.; Blondel, L.; Saugey, A.; Drenckhan, W. Simulating and interpretating images of foams with computational ray-tracing techniques. *Colloids Surf., A* **2007**, *309* (1−3), 159–176.
(41) Hoehler, R.; Sang, Y. Y. C.; Lorenceau, E.; Cohen-Addad, S. Osmotic Pressure and Structures of Monodisperse Ordered Foam. *Langmuir* **2007**, *24* (2), 418–425.
(42) Weaire, D.; Hutzler, S. *The Physics of Foams*; Clarendon Press: Oxford, 1999.
(43) Cervantes-Martinez, A. C.; Rio, E.; Delon, G.; Saint-Jalmes, A.; Langevin, D.; Binks, B. P. On the origin of the remarkable stability of aqueous foams stabilised by nanoparticles: link with microscopic surface properties. *Soft Matter* **2008**, *4* (7), 1531–1535.
(44) Guillermic, R. M.; Salonen, A.; Emile, J.; Saint-Jalmes, A. Surfactant foams doped with laponite: unusual behaviors induced by aging and confinement. *Soft Matter* **2009**, *5* (24), 4975–4982.
(45) Engl, W.; Backov, R.; Panizza, P. Controlled production of emulsions and particles by milli- and microfluidic techniques. *Curr. Opin. Colloid Interface Sci.* **2008**, *13* (4), 206–216.
(46) Private communication, Dr. Cosima Stubenrauch.